Fermi National Accelerator Laboratory

FERMILAB-Pub-83/91-EXP
7180.557
(Submitted to Phys. Rev. D)

A STUDY OF JET-LIKE STRUCTURE IN HIGH-TRANSVERSE-ENERGY EVENTS PRODUCED IN pp COLLISIONS AT 400 GeV/C

B. C. Brown, P. Devenski, H. Haggerty, and E. Malamud
Fermi National Accelerator Laboratory, Batavia, Illinois 60510

R. Abrams, H. Goldberg, C. Halliwell, F. Lopez, D. McLeod, and J. Solomon
University of Illinois at Chicago, Chicago, Illinois 60680

A. Dzierba, J. Florian, R. Heinz, J. Krider, H. Martin, P. Smith, S. Teige, and A. Zieminski
Indiana University, Bloomington, Indiana 47405

R. Ellsworth, R. Glasser, R. Holmes, P. Rapp, and G. Yodh
University of Maryland, College Park, Maryland 20742

and

S. Ahn and T. Watts
Rutgers University, New Brunswick, New Jersey 08903

November 1983

Operated by Universities Research Association Inc. under contract with the United States Department of Energy

A Study of Jet-like Structure in High-Transverse-Energy Events Produced in pp Collisions at 400 GeV/c

B. C. Brown, P. Devenski,[a] H. Haggerty and E. Malamud

Fermilab, Batavia, Illinois 60510

and

R. Abrams, H. Goldberg, C. Halliwell, F. Lopez,[b] D. McLeod, and J. Solomon

University of Illinois at Chicago, Chicago, Illinois 60680

and

A. Dzierba, J. Florian, R. Heinz, J. Krider, H. Martin, P. Smith, S. Teige and A. Zieminski[c]

Indiana University, Bloomington, Indiana 47405

and

R. Ellsworth,[d] R. Glasser, R. Holmes, P. Rapp and G. Yodh

University of Maryland, College Park, Maryland 20742

and

S. Ahn and T. Watts

Rutgers University, New Brunswick, New Jersey 08903

To be submitted for publication in Physical Review D

1. INTRODUCTION

We present in this paper results from Fermilab experiment E557 which studied the production of high transverse energy events in pp collisions at an incident momentum of 400 GeV/c. The goal of the experiment was to study production of jets in hadron-hadron interactions by employing a trigger that required a large amount of transverse energy ($E_t = \Sigma|p_t|$ for relativistic particles) to be deposited in a calorimeter with full azimuthal acceptance and large polar angle coverage. In our previous publication[1] we showed that such a trigger selects events that do not exhibit clear jet structure. Our results, which confirmed earlier observations of de Marzo et al.,[2] were recently supported by results from two other large acceptance experiments[3,4] performed in the same energy range. Experiments at the CERN ISR[4,5] and at the SPS collider[6,7] have established unambiguously copious production of jets in hadronic collisions at center of mass energies, $\sqrt{s}$, above 40 GeV. This suggests that large acceptance triggers, which adequately select jets at large $\sqrt{s}$, must at lower energies be complemented by additional constraints imposed on the data.

It is of interest to extend the energy range of jet studies to lower energies to understand how competing mechanisms obscure the jet signal when large acceptance triggers are used. With these aims in mind we have analyzed our data using relatively unbiased methods to select jet signals at lower energies.

The paper is organized as follows. Details of the apparatus and the triggers that were used are given in Section 2. The analysis of the calorimeter response is discussed in Section 3. In Section 4 we present yields as a function of E_t for various triggers. General properties of the data are discussed in Section 5.

In Section 6 we describe the search for jet-like structures in the data and discuss possible explanations for the failure of the large acceptance trigger to select jets and present results of analyses of events selected by various hardware triggers and software cuts. In Section 7 we discuss the properties of the jet-like events selected in the previous section. Our conclusions are presented in Section 8.

Throughout this paper an emphasis will be put on new experimental results. However to illustrate the trends observed in the data we will occasionally compare the data with the predictions of two different models: a Longitudinal Phase Space model (LPS) and a QCD-gluon bremsstrahlung model (QCD).[8] The comparisons will enable us to estimate the effects of energy-momentum conservation in large multiplicity events (comparison with the LPS model) and to search for jet-like structures in the data (comparison with the QCD model). We will limit model comparison to the event structure only because of the large uncertaintities, both experimental and theoretical, in the absolute normalization of cross sections. The models are described in Section 6.

2. APPARATUS

The experimental procedure as well as details of the apparatus have already been described in our previous publications.[1,9] We describe here the main features of the experiment relevant to the present analysis.

The layout of the apparatus is shown in Fig. 1. The experiment was performed using 400 GeV diffractively produced protons in the M6W beam line at Fermilab. The apparatus consisted of the Fermilab multiparticle spectrometer.[10] A typical beam intensity of 0.5×10^6 protons was spread over a 1.0s spill, which occurred once every 10 seconds. The beam was incident on a 45-cm H_2 target followed downstream by two interchangeable metal foils of Al, Cu or Pb[9] sufficiently thin that rescattering effects were negligible. Multiwire proportional chambers (34

planes of 8500 wires) and magnetostrictive spark chambers (24 planes) detected charged particles. Particle momenta were measured using a spectrometer magnet that provided a 0.2 GeV/c p_t kick. Downstream of the tracking chambers was placed a 2.3 x 3.1 m^2 highly segmented calorimeter[11] consisting of 280 modules arranged into three sections (see Fig. 1). The upstream section which consisted of 126 lead-scintillator sandwiches (16 radiation lengths, L_r, and 0.8 absorption length, L_a) primarily measured the energy of electrons and photons (see Fig. 2). This electromagnetic section was followed by two hadronic sections of 126 and 28 iron-scintillator sandwiches respectively ($6\lambda_r$ and $7.5\lambda_a$ combined). The distance from the center of the hydrogen target to the front face of the calorimeter was 9.4 m. The energy resolution of the calorimeter was measured to be $\sigma/E = 0.2/\sqrt{E}$ for electrons and $\sigma/E = 0.7/\sqrt{E}$ for hadrons, where the energy E is measured in GeV.[11] The calorimeter served both as a trigger (see below) and as a detector of neutral and charged particles (see Section 3).

The geometrical acceptance of the apparatus was complete in azimuth for the polar angle range $59° < \theta^* < 114°$ as measured in the proton-proton center-of-mass frame (Fig. 2a). The overall acceptance was estimated to be equivalent to 2π azimuthal acceptance for $47° < \theta^* < 125°$. This corresponds approximately to a c.m. rapidity range, $-0.65 < y^* < 0.84$.

The apparatus was triggered in several ways. First an inelastic collision was detected by one of two methods. An incident proton was required to miss a counter of 1 x 1 inch squared (designated 1 x 1 in Fig. 1) placed on the beam line 7.5 meters downstream of the target, or a large pulse height ($\geq$ 2 times minimum ionizing) was required to be registered in a counter (designated DEDX in Fig. 1) placed immediately downstream of the target. This constituted the "interacting-beam trigger" and was sensitive to approximately 90% of the total inelastic pp cross section. The other triggers consisted of this trigger with an

additional requirement that at least a certain amount of transverse energy was present in some preset region of the calorimeter. For all the triggers the incident proton was required to be unaccompanied by another beam particle within ±130 ns. Pulse height information from a scintillation counter was used to eliminate rf buckets containing more than one particle. The rf buckets were 2 ns wide and were separated by 20 ns. A final veto on a following interaction occurring within ±200 ns was imposed.

To form the calorimeter transverse energy trigger the output from each module was weighted by the sine of the polar angle that the module subtended at the target. E_t sums for several different configurations of calorimeter modules were formed simulataneously. Data from three configurations are presented in this paper: full azimuthal acceptance ("global trigger") and two limited $\Delta\phi$ small aperture with approximate acceptances of 7.8, 1.65 and 0.70 sr respectively as measured in the proton-proton center-of-mass frame (see the shaded areas of Fig. 2b).

Data were collected with several E_t thresholds for each type of high E_t trigger. The absolute E_t scale from the calorimeter was determined by calibrating before and after the 18-day data run. In both cases a 20-GeV/c beam of electrons and hadrons was directed into each module. A 10% shift in the responses of individual modules typically occurred between the two calibrations. This shift was found to be consistent with the results of a laser monitoring system and with the observed time dependence of trigger rates. The variation of module responses was taken into account by assuming a linear dependence of the module gains with time between the two calibrations runs. The response of the electromagnetic section of the calorimeter was found to be 17% larger for incident electrons than for hadrons. This effect was included by organizing module responses into electromagnetic and hadronic energy clusters (see next Section).

In this analysis the spectrometer was used only to determine the position of the interaction vertex. The vertex resolution was σ = 4 mm as measured along the incident beam direction. This provided a clean hydrogen, nuclear-target separation.[9] The E_t sums for a given event were recalculated using the exact vertex position. A Monte Carlo simulation, based on the observed spectra of particles, was employed to unfold the energy resolution, energy leakage and granularity of the calorimeter and to correct for the effects of the magnetic field. The total uncertainty of the E_t scale from the calibration and these sources was estimated to be $\sigma(E_t)/E_t$ = ±5%.

The pp interactions used in this analysis consisted of (32, 16 and 6) x 10^3 events taken with the interacting-beam, global and limited $\Delta\phi$ triggers, respectively. They were selected by requiring an interaction vertex to be within the 40 cm long fiducial volume of the H_2 target. In addition, the observed E_t was required to exceed the hardware threshold by at least 1 GeV transverse energy. The integrated luminosity for the global and limited $\Delta\phi$ trigger data sets was 4 and 2 nb^{-1}, respectively.

3. ANALYSIS

Much of the analysis presented in this paper was performed using the calorimeter module outputs directly. This was appropriate for studying yields and general event structure. To perform more detailed studies (e.g. multiplicity of secondaries, jet reconstruction etc.) it was necessary to organize the responses of the calorimeter modules into energy clusters henceforth known as "calorimeter tracks". The cluster forming algorithm first combined the responses of corresponding electromagnetic and hadronic modules to form responses of "dual-modules". The dual-module with the largest response was then found. This dual-module, together with all adjacent dual-modules, formed a group whose responses contributed to the energy of a cluster. Energy was assigned to a cluster by comparing the actual energy deposition within the group with the predictions of a shower simulation.[12] The center of a shower (cluster) was obtained by averaging the positions of the centers of dual-modules within the group weighted by the squares of their responses. The cluster was designated to be electromagnetic or hadronic depending on its energy deposition pattern in the electromagnetic and hadronic calorimeters. Modules whose responses were badly inconsistent with the predictions of the shower simulation were removed from the group and a new prediction was made. The difference between the actual module responses and the predictions from the shower simulation was then calculated and the procedure was repeated for the next remaining dual-module with the highest energy. This procedure was repeated until clusters with energy less than 1 GeV remained; these were ignored. The effects of the systematic errors due to the cluster finding algorithm are discussed in Section 5.

We have found the multiplicity of electromagnetic tracks so formed to be greater than half of the hadronic multiplicity. Electromagnetic tracks presumably contain a mixture of resolved photons and unresolved neutral pions and hence are unsuitable for calculating π° and η° multiplicities. Therefore we do not compare production rates for electromagnetic tracks with the known π° and η° inclusive cross sections; we will concentrate instead on the comparison of hadronic track production rates.

Hadronic tracks consist mainly of charged pions with a few percent addition of charged and neutral kaons. In Fig. 3 we compare the E_t spectrum of hadronic calorimeter tracks detected between 60° and 120° as measured in the center-of-mass frame with relevant inclusive cross sections measured in other experiments.[13,14] The hadronic track data agree to within 20% with published cross sections over a wide p_t range ($0.5 < p_t < 5$ GeV/c). This agreement gives us confidence in the performance of our cluster finding algorithm and in the calibrated E_t scale of the

experiment. In Fig. 4 we compare multiplicity distributions of the hadronic tracks with charge particle data obtained in another pp experiment using a similar center-of-mass energy and an apparatus with a similar rapidity acceptance.[15] The difference between Ref. 15 data and E557's data could be greatly reduced if corrections were made for Ref. 15's incomplete azimuthal acceptance (90% of 2π) and the detection of neutrons and K_L^o's in E557's calorimeter. We conclude that typical hadronic multiplicities (of, say, 15) are known to ±2. We also note that there is no indication of substantial merging of hadronic tracks in large multiplicity events.

Even though electromagnetic tracks did not correspond to single photons, they were still used extensively to form variables that were not sensitive to this fact (eg. the formation of total E_t).

4. YIELDS

It has been previously shown that E_t yields vary strongly with the acceptance of the apparatus.[1][2] For those studies a large range of acceptances was used ($7.8 < \theta^* < 0.7$ sr). In order to see if this trend still exists when a small range of acceptances are used, the yields from the two limited $\Delta\phi$ calorimeter sectors (denoted A and B in Fig. 2b) are compared in Fig. 5. An increase of a factor of 2.3 in acceptance causes a change of approximately 10 in yield. This is an indication that the secondaries hitting the calorimeter within the trigger acceptance are distributed throughout the entire aperture of the triggering sector and little collimation of secondaries is occuring within it. There is also no indication of the yields exhibiting a power-law dependence on E_t. Such a variation would be expected if a hard-scattering process was dominating the production mechanism.

Yields for small acceptances were obtained by an alternative method using solely the data obtained when the global trigger was used. For each event the

E_t within the geometrical areas of Sectors A and B was calculated off-line. Since the data were collected using various global E_t thresholds the number of events within a given E_t bin, dN/dE_t, did not correspond to the measured cross section $d\sigma/dE_t$. In order to restore this correspondence events were given appropriate weights, $w = (d\sigma/dE_t)/(dn/dE_t)$. The results are shown in Fig. 6 where they are compared with the results presented in Fig. 5. The two sets of data agree to within a factor of ~2. The tendency for the two data sets to disagree at higher values of E_t is probably due to the different methods for correcting the raw data yields. The analysis of the hardware triggered data summed the calorimeter module responses within the trigger sector. The observed yield was then corrected for energy leakage out of and into the given sector. The size of the correction depended on the details of the shower simulations and on the assumed distribution of secondaries. The correction was of a statistical nature; it could not be applied to individual events. In contrast to this the analysis of the global data used calorimeter tracks which were formed by gathering energy from several modules. Occasionally the energy from a module outside a sector would be used to form a cluster whose center was within a sector. Similarly energy from a module within a sector could be used to form a cluster whose center was outside. In this case the energy leakage into and out of the sector was corrected on an event by event basis.

We conclude from this comparison of yields that the systematic errors present on the small acceptance data cause a factor of ~2 uncertainty in the measured cross section. We note that present theoretical predictions for the high-E_t rates are also subject to similar or even larger uncertainties. We therefore conclude that our global data can be used with software cuts to simulate reduced aperture triggers.

In an attempt to decrease the systematic error discussed above and to facilitate comparison with theoretical predictions we have used the global data to produce cross sections in well defined θ^* and ϕ regions. The θ^* acceptance (assuming massless secondaries) was restricted to the range $120° > \theta^* > 60°$ as shown in Fig. 2(a). Energy that was detected within the calorimeter but outside the θ^* range could still contribute to clusters within the θ^* range. This cut on θ^* was made to diminish the effects of energy leakage out of the fiducial area.

The chosen polar angle range had the advantage that it allowed one to perform symmetry checks on the data. Two pie-shaped back-to-back sectors were formed with each sector subtending $\Delta\phi = 45°$ in azimuth. The sectors were situated in the up-down and left-right configurations as viewed along the incident beam direction. A comparison of yields showed a difference of a factor of 2 for the two configurations (this was after magnetic field kick corrections). In addition yields from the polar angle region $60° < \theta^* < 90°$ were compared with those from $90° < \theta^* < 120°$. They agreed to within a factor of 2 also. We conclude, as before, that yields can be trusted typically to a factor of 2.

Yields from various sized pie-shaped sectors are plotted in Fig. 7. The characteristics seen previously from hardware-triggered sectors are plainly visible: the increasing dependence on E_t with decreasing acceptance and the strong dependence on aperture size. One can also see that no deviation from an exponential variation occurs at high values of E_t even for small ($\Delta\phi = 11.25°$) sized sectors.

5. GENERAL PROPERTIES OF EVENTS

In this section we describe general properties of events obtained using the global trigger and discuss their dependence on E_t.

The transverse energies of individual tracks were summed to form total electromagnetic and hadronic transverse energies separately. The ratio of these two types of transverse energies decreased from 0.8 for $E_t < 4$ GeV values (E_t is the sum of the two types of transverse energy) to 0.35-0.45 at $E_t = 10$ GeV; above 10 GeV it remained constant. The relative importance of electromagnetic energy at large angles for low E_t events is qualitatively predicted by the longitudinal phase space model (LPS). Also the observed value of the electromagnetic to hadronic E_t ratio at high E_t values is in a reasonable agreement with the model predictions. However the experimental value of the ratio is subject to a large systematic error due to uncertantities of the cluster forming algorithm; specifically, two calorimeter tracks, one hadronic, one electromagnetic could be formed occasionally when only a single hadronic track really existed. To estimate the systematic error due to this we have forceably merged closely spaced tracks. The result was that the ratio dropped by 0.10. We consider this change to represent a systematic error for the discussed ratio. We note that such a systematic error has a small effect on hadronic multiplicities and causes the average transverse energy of a hadronic track to be changed by 100 MeV.

In Fig. 8 we show the variation of average hadronic calorimeter track multiplicity detected in the calorimeter with total transverse energy and compare it with the predictions of the LPS and QCD models. No E_t cut (other than their energy being greater than 1 GeV) and no acceptance cuts have been applied to the calorimeter tracks. As expected an increase in multiplicity with total E_t occurs. The rate of increase appears to lessen as E_t is increased; this is reminiscent of an effect reported previously.[2] One can see that the predictions of both models are in good agreement with data in the range $E_t < 11$ GeV. Above 11 GeV the LPS model predicts a larger multiplicity than the data. This is a direct consequence of limiting the transverse moments of the secondaries in the model.

Even though there is an increase in hadronic multiplicity with E_t, it is not strong enough to maintain the ratio of transverse energy to hadronic cluster multiplicity at a constant value. This is shown in Fig. 9. The average ratio approaches 0.7 GeV/c for events with high total transverse energy in agreement with that reported at 300 GeV for pp and π^-p interactions (~ 0.65 GeV[2]). From Fig. 9 one can see that the QCD model predicts the increase of this ratio with E_t.

From Figs. 8 and 9 we conclude that high transverse energy events typically have a large number of secondaries with each particle individually having a relatively small amount of transverse momentum.

Event structure was studied in more detail in terms of the planarity variable [1,2] which was calculated in the transverse plane of the event. In this projection an event axis was chosen arbitrarily and the p_t vector for each calorimeter track was decomposed into components parallel and transverse to this axis. Denoting the sum of the squared components along and transverse to the event axis as A and B, then planarity is defined as $P = (A-B)/(A+B)$. P was then maximized by varying the direction of event axis. For pencil-like back-to-back jets, P approaches 1 while for isotropic events with large multiplicity it approaches 0. Figs. 10(a) and (b) show the observed planarity distributions for events with $7 < E_t < 14$ GeV and $E_t > 14$ GeV respectively for the global data sample (similar distributions were obtained directly from using calorimeter module responses). It is clear that the majority of the events are non-planar. This is summarized in Fig. 11a where the average planarity as a function of E_t in shown. In addition the fraction of high planarity events ($P > 0.7$) with high values of E_t is equal to 9% and remains constant. This is shown in Fig. 11b.

In order to see whether the high planarity events are primarily due to fluctuations of typical events we used the experimental data themselves rather than the predictions of the LPS model since the simulation of these rare events

would depend heavily on the specific input parameters of the model. Using the experimental data overcomes this objection. We randomized the directions of all of the calorimeter tracks independently in the transverse plane (their polar directions were preserved). Consequently, any spatial correlations between particles were destroyed. The randomization procedure was repeated until the magnitude of the original p_t imbalance measured in the calorimeter was reproduced to within ±2% (the results did not change significantly when this requirement was relaxed to ±25%). Planarity was then recalculated using the randomized calorimeter tracks. By performing this randomization we aim to study how the event structure is constrained from energy-momentum conservation alone.

The effect of this analysis is shown in Fig. 12 where the transverse energy flow for events with $E_t > 14$ GeV is plotted. The original data are compared to the randomized tracks. Even though two small excesses exist, one near the track with maximum transverse energy ($\phi = 0°$) and one opposite to it ($\phi = 180°$), from the sizes of the excesses we conclude that the structure of a typical high E_t event is governed primarily by energy-momentum conservation.

However, from Fig. 10(a) and (b) one can see that a deficit of high planarity randomized events is produced indicating that high planarity events are not totally caused by statistical fluctuations of low planarity ones. The excess of original high planarity events above those produced by the randomization procedure increases strongly with total E_t. This is shown in Fig. 13. This increase is in contrast to the constancy of the fraction of original high planarity events shown in Fig. 11b. We conclude from Fig. 13 that approximately 40% of events with $E_t > 14$ GeV and $P > 0.7$ are caused by dynamical effects other than statistical fluctuations of large multiplicity low p_t events.

6. SEARCH FOR JET-LIKE STRUCTURES

In order to search for jet-like structures within the global and limited $\Delta\phi$ data sets we performed several cuts. It is apparent from arguments presented in the previous section that one of the most fundamental would be E_t requirement. This view is supported by the theoretical work of Akesson and Bengtsson[16] who have made a quantitative prediction for the minimum value of E_t above which hard scattering should become the dominant process for a given aperture. According to these authors the cross-over value of E_t is equal to

$$E_t^{co} = 16 \cdot \Delta y \cdot \Delta\phi/2\pi \quad [GeV],$$

where Δy is the rapidity interval and $\Delta\phi$ the azimuthal angle interval included in the trigger (the value of E_t^{co} is, to first approximation, independent of the c.m. energy squared of the colliding particles). For this experiment one would not expect to see jets dominating the global data for events with the values of E_t below 24 GeV. This is not in disagreement with the jet signal presented in the previous section which constituted only 5% of <u>total</u> data with $E_t > 14$ GeV. For the limited $\Delta\theta^*$ acceptance data one would expect jets to dominate above 15 GeV.

Several theoretical models offer explanations for the lack of jet dominance in the events selected with a global trigger.[8,16-20] Processes that might obscure the jet signal essentially fall into three categories:

- contribution to the measured transverse energy from fragments of spectator jets[17,18]
- gluon bremsstrahlung before and after the hard scatter[8,18,19]
- two competing processes: a large multiplicity tail of low-p_t type collisions and hard scatters, with the relative contribution of the two processes depending on the aperture of the calorimeter trigger[16,20].

The results from several previous experiments suggest suitable cuts on the data. For example, a large aperture experiment at the ISR[5] has reported the emergence of jets when triggered on electromagnetic component of transverse energy alone. A Fermilab experiment[21] combined a requirement of large global E_t with restricted multiplicity or with the presence of two or more energetic clusters[3,22] (so called 'two-high' triggers[3]).

In order to select jet-like events from the background of competing processes we studied events selected by hardware and software triggers with:

A. limited aperture in the azimuth;

B. limited aperture in the polar angle;

C. a modified 'two-high' trigger requirement;

D. limited particle multiplicity in the final state;

E. electromagnetic or hadronic E_t dominating the global E_t;

F. a transverse energy cut on the secondaries.

The data presented in this section are compared with predictions of the LPS and QCD models.

The LPS model takes into account the leading nucleon effect and correctly reproduces multiplicities and p_t-spectra of particles as known from bubble chamber experiments.[23] It also includes a long tail of large multiplicities in the multiplicity distribution which for $n_{ch} > 28$ is generated according to an exponential form $\exp(-3n_{ch}/\langle n_{ch}\rangle)$, where n_{ch} and $\langle n_{ch}\rangle$ are the charged particle multiplicity and the average value, respectively. In this model particles are produced in an uncorrelated fashion except for strict energy-momentum conservation which is imposed for each generated event. The model does have its limitations; it predicts an average transverse momentum for the secondaries which does not vary with event E_t. This is in disagreement with the data (See Fig. 9). There-

fore we will use this model with caution; it will be primarily used to estimate the effects of energy-momentum conservation.

The QCD model represents an upgraded version of the 4-jet model.[24] It takes into account gluon bremsstrahlung from the initial and scattered partons. The final state quarks (gluons decay into $q\bar{q}$ pairs) are organized into colorless pairs and fragmented into hadrons according to either the Field-Feynman scheme[25] or phase space depending on the invariant mass of the pair. The spectator quarks from the initial hadrons are treated in the model as single partons.

In our calculations we have used standard values of parameters as suggested by the authors of Ref. (8), except for the after-scatter beam cutoff, t_A^{min}, which value has been changed from 3 to 1 $(GeV/c)^2$. Only hard scatters with $p_t >$ 1.5 GeV/c were considered. However, most of the model predictions for event structure are insensitive to this cutoff. The parameters of the models have been taken from the literature and have not been "tuned" to optimize agreement with our data.

A. The limited $\Delta\phi$ aperture data

For this analysis we have selected data triggered by a deposition of E_t in sector A of the calorimeter (see Fig. 2(b)).

The average planarity, <P>, calculated using module responses from the entire calorimeter, increases monotonically with the transverse energy detected in the triggering sector (Fig. 14), indicating that events become more jet-like with increasing E_t. This increase is mainly due to the collimation of particles within the triggering sector. The increase for E_t values above 4 GeV is predicted by the QCD model whereas the LPS model predicts the rise at low E_t.

The transverse energy flow as measured by the whole calorimeter is plotted in Fig. 15 as a function of azimuthal angle, (ϕ = 0 is defined as the center of the triggering sector). The low E_t data agree well with predictions of the LPS model. For data with medium E_t ($4 < E_t < 5$ GeV) both the LPS and QCD models predict the general trends of the data; the QCD model is in better agreement with measured energy flow within the triggering sector ($\Delta\phi$ = 0° to 30°). This is seen to be so also for the high E_t data.

To study in greater detail the collimation effect within the triggering sector we follow Ref. 4 and introduce the variable pseudothrust, T, defined as:

$$T = \sum_i |\hat{e}\cdot\vec{p}_{ti}| / \sum_i |\vec{p}_{ti}| \quad , \tag{3}$$

where the sums are carried out over the modules in the triggering sector and $\hat{e}$ is a unit vector along the direction of $\sum_i \vec{p}_{ti}$. The experimental size of the triggering sector limits the range of T to values from 0.85 (two maximally separated tracks) to 1 (pencil-like jets). The fraction of events with T > 0.96 rises as a function of E_t (see Fig. 16). This is similar to the effect seen in Fig. 14 and once again the QCD model is successful in predicting the increased collimation at high values of E_t. The LPS model is unable to account for this effect because of the model's method of producing large values of E_t. It does so by producing a large number of low p_t secondaries randomly in azimuth.

We notice that a collimation effect on the trigger side (ϕ = 0°) does not lead to a detectable increase in collimation on the side opposite to the triggering sector (ϕ = 180°). Transverse energy flows for low- and high-T events are very similar (Fig. 17). Both energy flows agree well with QCD predictions.

Results for the limited $\Delta\phi$ trigger presented here were obtained for events selected by a hardware trigger. We obtain similar distributions from a software acceptance cut imposed on the global data. We conclude that the global data with software cuts can be used not only to derive cross sections for smaller apertures as shown in Section 3 but also to study event structure in detail. This will be used extensively in the following analyses.

B. The limited θ^* aperture data

For this analysis we used exclusively the pulse height information from the calorimeter modules. We have introduced software acceptance cuts on the global data. The global trigger acceptance was reduced to approximately $63^\circ < \theta^* < 110^\circ$ ($\Delta\Omega^* = 5.0$ sr), as shown in Fig. 2(c).

The event structure does not change with E_t when no acceptance cuts are applied to the global data[1] (See Fig. 11). The "reduced" global data obtained by applying the above cut do however exhibit a statistically significant shift towards larger planarity values for $E_t > 12$ GeV. This is shown in Fig. 18 where planarity distributions (using modules from the entire calorimeter) are shown as a function of E_t (calculated using modules from the limited acceptance alone). The increase in the number of high planarity events is emphasized in Fig. 19 where the average planarity and the fraction of high planarity events is shown as a function of E_t (calculated as before). A comparison with the LPS and QCD model predictions is also shown. As noted in the limited $\Delta\phi$ analysis, the LPS model does not predict the increased collimation. In contrast to this the QCD model predicts a substantial increase in planarity at high values of E_t.

We note that the QCD model also predicts increasingly planar events for events detected using the full calorimeter acceptance (see Fig. 11). We conclude from a comparison of Figs. 11 and 19 that decreasing the polar acceptance of the calorimeter diminishes the non-jet like event structure present in the experimental data. The source of this structure could be for example, beam and target fragments.

The increase of $\langle P \rangle$ is also observed when $\langle P \rangle$ is calculated using only those modules which are included in the restricted acceptance. Both effects are also present when calorimeter tracks rather than module responses are used. The increase in $\langle P \rangle$ is therefore not due to effects such as granularity of the calorimeter.

C. Modified 'two high' trigger

This analysis was based on software cuts imposed on the global data and it also used calorimeter module responses.

We have divided the calorimeter into eight regions (see Fig. 2(d)) each covering approximately $\Delta\phi = 90^\circ$ and $\Delta\phi^* = 35^\circ$ with $\Delta\Omega^*$ ranging from 0.9 sr to 1.2 sr. In addition to demanding a high value of E_t in the entire calorimeter we required the value of transverse energy in two of the eight groups to exceed a certain threshold, E_t^{thr}. Since there was no constraint on the relative alignment of these two chosen groups, any of the 28 combination of pairs may occur. Only eight of these combinations correspond to kinematically favored 'back to back' and 'back-antiback' configurations in the ϕ and θ^* angles. In Fig. 20 we plot the fraction of global E_t triggers fulfilling the additional 'two-high' requirement as a function of E_t^{thr}. A 3 GeV cutoff selects only 5% of all events with $E_t > 12$ GeV, 70% of which correspond to 'back to back' or 'back to antiback' configurations. The LPS model predicts this trend well indicating that such event structure is dominated by energy-momentum considerations rather than jet production. This is confirmed in Fig. 21 where the average planarity of events selected by this method increases with E_t^{thr}. We conclude that there is no overwhelming evidence that a "two-high" type trigger unambiguously selects events caused by hard scattering.

D. Limited particle multiplicity in the final state

For this analysis we used hadronic calorimeter tracks rather than module responses; no acceptance cuts were applied to the data. The multiplicity and planarity were determined for each event. Average planarity values for low and high multiplicity events were then plotted (see Fig. 22). The increase in planarity for low multiplicity events confirms a result reported earlier[21,22] using all calorimeter tracks, electromagnetic and hadronic. The difference be-

tween the mean planarities for low and high multiplicity events is partially due to the correlation between planarity and multiplicity and is at least qualitatively predicted by both the LPS and the QCD models. Consequently, it is difficult to asses whether the increase at high E_t is due mainly to kinematic effects or has a deeper dynamic origin.

E. Electromagnetic and hadronic components of global E_t

In Section 3 we described how a calorimeter track was designated to be electromagnetic (em) or hadronic (had). The transverse energies of the individual tracks were summed to form total electromagnetic and hadronic energies separately (E_t^{em} and E_t^{had} respectively). The sum, $E_t^{em} + E_t^{had}$, was equal to the total transverse energy in the event, E_t.

In Fig. 23(a) we show the dependence of average planarity (calculated using all tracks) as a function of E_t^{em} rather than total E_t. One sees a rise in planarity for E_t^{em} values above 6 GeV. A similar trend has already been reported by an ISR experiment[5]. A significant rise in the average planarity value is also observed as a function of E_t^{had} (Fig. 23(b)). This is the first time that such a rise has been seen as a function of hadronic transverse energy.

We have checked this result by studying how the average planarity varies as a function of transverse energy deposited in the electromagnetic calorimeter modules (rather than using calorimeter tracks). A similar effect is seen and we conclude that the effect is not introduced by the algorithm that forms and separates electromagnetic and hadronic tracks.

In an attempt to understand the origin of the effect we have divided events with a given total E_t into three categories: those with a dominant fraction of electromagnetic energy ($E_t^{em}/E_t > 0.6$), those with a dominant hadronic energy ($E_t^{had}/E_t > 0.8$) and the remaining events ($0.2 < E_t^{em}/E_t < 0.6$). The fraction of events with $E_t^{em}/E_t > 0.6$ ($E_t^{had}/E_t > 0.8$) increases with E_t^{em} (E_t^{had}), as expected

from simple kinematic constraints. Therefore we might expect the increase of $\langle P \rangle$ with E_t^{em} or E_t^{had} observed in Fig. 23, to reflect the difference between mean planarities for events with large and medium values of the ratio E_t^{em}/E_t (E_t^{had}/E_t), respectively.

In Fig. 24 we plot average planarity as a function of total E_t for the three categories of events. Indeed at all values of E_t events dominated by one type of energy have larger values of average planarity than the more balanced events. The difference between the average planarities for the two data sets is constant as a function of E_t (see Fig. 25) up to $E_t \approx 17$ GeV and only then starts to increase.

Events dominated by one type of energy are characterized by smaller total particle multiplicites than the remaining events. This fact is consistent with the positive correlation between charged and neutral pion multiplicities[27] known from low-p_t physics. However it is not clear to what extent the observed correlation between $\langle P \rangle$ and the ratio E_t^{em}/E_t (E_t^{had}/E_t) reflects correlations between planarity and particle multiplicity discussed in the previous section. The LPS model fails to predict an increase of $\langle P \rangle$ with E_t^{em} or E_t^{had}. The model correctly reproduces the difference between $\langle P \rangle$ for balanced and unbalanced events up to $E_t \lesssim 10$ GeV, but contrary to the data, predicts the difference to disappear with E_t.

We have also calculated two additional values of the planarity variable for each event using electromagnetic and hadronic tracks separately and studied their dependence on the corresponding type of transverse energy. The increase of average planarities of a given type at large transverse energies was found to be statistically insignificant.

F. E_t cut on secondaries

The increase in planarity observed in events that were restricted to limited acceptances (in ϕ or θ^*) is suggestive of a reduction of a possible source of "soft" background. This could also be the explanation of the increased planarity for constant multiplicity events. To investigate this further we have attempted to minimize the effect of low p_t secondaries by imposing the requirement $p_t >$ 0.5 GeV/c on all calorimeter tracks. The resulting variation of average planarity with event E_t is shown in Fig. 26. No increase in planarity is observable for high E_t events; in fact little change occurs in the event structure when such a cut is applied (c.f. Fig. 11).

There is also no indication of an increase with E_t in the fraction of total E_t carried by the most energetic or two most energetic calorimeter tracks (Fig. 27). An increase has been observed at higher energies[4-7]. However the 'clusters' used in refs. (4-7) correspond in size to jets rather than to single particles as in the case in our analysis. The observed trend in our data is in agreement with the predictions of both the LPS and QCD models.

From the studies described in this section we conclude that the data show a strong indication for the emergence of jet-like event structure even at the low incident momentum of 400 GeV/c. Several different cuts on the data (restricting the azimuth or polar angle acceptance of the apparatus, limiting the particle multiplicity, dividing events into electromagnetic and hadronic portions) produce effects that cannot be described by an extrapolation of uncorrelated low-p_t phenomena. We interpret this as evidence for the onset of jet production ($E_t > 14$ GeV).

7. PROPERTIES OF PLANAR EVENTS

In order to study the properties of events with planarity values greater than 0.7 we formed several variables using the transverse momenta associated with the calorimeter tracks.

Firstly we formed for each hadronic calorimeter track the variable $x_p = 2E_t^{had}/E_t$ where E_t^{had} was the transverse energy of the track and E_t was the total energy detected in the calorimeter. From Fig. 28 we see that the x_p distribution for low and high planarity events differ considerably. In Fig. 28(c) a comparison is made with the scaled hadron energy spectrum from e^+e^- annihilations at 14 GeV center-of-mass energy.[28] One can see that the high planarity events from this experiment resemble the two-jet events produced in e^+e^- collisions. The E557 data do lie systematically below the e^+e^- distributions by almost a factor of 2 but this is probably due to the calorimeter registering only a fraction of the away side jet, contrary to the e^+e^- situation, where both jets are recorded (one can see this effect in the transverse energy flow plots e.g. Fig. 15). Therefore the x_p distributions from this experiment are expected to have lower multiplicities.

The QCD model correctly reproduces the changes in the character of the distribution with increasing planarity, but overestimates the density of energetic particles for $P > 0.7$ (see Fig. 28(c)).

In Fig. 29 we show how high planarity ($P > 0.7$) events change in structure as E_t is increased. At low E_t ($E_t < 7$ GeV) the x_p distribution is strongly affected by single particles ($x_p = 1$); from $E_t = 7$ to 20 GeV only a small change in structure occurs. The slight "softening" of the distribution is in agreement with data from a previous experiment.[10]

We have investigated the jet structure within an event by dividing the event into two halves in the transverse plane. To do this an axis perpendicular to the planarity axis was used. Then, vector sums of the calorimeter tracks momenta were formed. The directions of these sums formed, by definition, the two jet directions. The distribution of the projection of calorimeter tracks momenta onto the jet direction was very similar to the x_p distributions. The distribution of the tracks momenta perpendicular to the jet direction is shown in Fig. 30. It can be seen that the high planarity events are more collimated, as expected. One can see that "jets" from this experiment appear to be somewhat wider than those seen in 14 GeV center-of-mass energy e^+e^- collisions.[29]

8. SUMMARY

We have presented results from an experiment which studied the production of high transverse energy events in pp collisions at a center-of-mass energy of 27.4 GeV. Only a small fraction of events exhibit jet-like structure. We have estimated that approximately half of those events are caused by dynamical effects other than statistical fluctuations of large multiplicity low-p_t events.

We have imposed several different restrictions on the data in order to select an unbiased sample of events with jet-like structure. Many of the cuts e.g. restricting the azimuth or polar angle acceptance of the apparatus, limiting particle multiplicity, dividing events into electromagnetic and hadronic portions produce effects that cannot be described by an extrapolation of uncorrelated low-p_t phenomena. On the other hand many aspects of the data agree qualitatively with the predictions of the QCD-gluon bremsstrahlung model. We conclude therefore that the data show an indication for the emergence of jet-like event structure even at the incident momentum of 400 GeV/c. However, due to large background, a more quantitative separation of jet signal remains very model dependent.

We are grateful for the excellent technical support given to us by the multiparticle spectrometer facility group led by Dan Green and by all the technical shops situated in the institutions that participated in this experiment. This work was supported in part by the U.S. Department of Energy and the National Science Foundation.

(a) Present address: Higher Institute for Chemistry and Technology, Sofia, Bulgaria.

(b) Present address: Florida State University, Tallahassee, FL. 32306.

(c) On leave of absence from University of Warsaw, Warsaw, Poland.

(d) Present address: George Mason University, Fairfax, Va. 22030.

REFERENCES

1. B. Brown, et al., Phys. Rev. Lett. 49, 711 (1982).
2. C. De Marzo et al., Phys. Lett. 112B, 173 (1982), and Nucl. Phys. B211, 375 (1983).
3. M. Arenton et al., in Proceedings of the 21st High Energy Physics Conf., Paris, edited by P. Petiau and M. Porneuf, Les Edition de Physique Paris, 1982, p. C3-131 (1982).
4. T. Akesson et al., Phys. Lett. 128B, 354 (1983).
5. A. L. S. Angelis et al., Phys. Lett. 126B, 132 (1983).
6. M. Banner et al., Phys. Lett. 118B, 203 (1982).
7. G. Arnison et al., Phys. Lett. 123B, 115 (1983).
8. G. C. Fox and R. L. Kelly, LBL-Caltech Report Nos. LBL-13985, CALT-68-890 (1982), R. D. Field, G. C. Fox and R. L. Kelly, Phys. Lett. 119B, 439 (1982).
9. B. Brown et al., Phys. Rev. Lett. 50, 11 (1983).
10. C. Bromberg et al., Nucl. Phys. B171, 1 (1980).
11. P. Rapp et al., Nucl. Instr. Methods 188, 285 (1981).
12. M. della Negra, Phys. Scripta 23, 465 (1981).
13. F. E. Taylor et al., Phys. Rev. D14, 1217 (1976).
14. D. Antreasyan et al., Phys. Rev. D19, 764 (1979).
15. T. Akesson et al., CERN preprint EP/83-75, to be published in Nucl. Phys. B.
16. T. Akesson and H. U. Bengtsson, Phys. Lett. 120B, 233 (1983).
17. R. Singer et al., Phys. Rev. D25, 2451 (1981).
18. R. Odorico, Phys. Lett. 118B, 151 (1982) and Univ. of Bologna preprint IFUB 82/20, 1982.
19. M. Greco, Phys. Lett. 121B, 360 (1983).
20. F. Bopp and P. Aurenche, Z. F. Phys. C13, 205 (1982).
21. C. Halliwell, in Proceedings of the 13th Multiparticle Symposium Volendam, p. 509 (1982) edited by W. Kittel, W. Metzger and A. Stergiou.

References (continued)

22. T. L. Watts, in Proceedings of the 13th High Energy Physics Conf., Paris, edited by P. Petiau and M. Porneuf, Les Editions de Physique, Paris 1982, p. C3-127.
23. C. Bromberg et al., Phys. Rev. Lett. 31, 1563 (1973) and Nucl. Phys. B107, 82 (1976).
24. R. P. Feynman, R. D. Field and G. C. Fox, Phys. Rev. D18, 3320 (1978).
25. R. D. Field and R. P. Feynman, Nucl. Phys. B136, 1 (1978).
26. T. Akesson et al., Phys. Lett. 118B, 185 (1982), and 123B, 133 (1983).
27. R. D. Kass et al., Phys. Rev. D20, 605 (1976).
28. R. Brandelik et al., Phys. Lett. 114B, 65 (1982).
29. R. Brandelik et al., Phys. Lett. 86B, 243 (1979).

FIGURE CAPTIONS

1. The Fermilab Multiparticle Spectrometer. $\hat{C}_A$ and $\hat{C}_B$ are two multicelled Cerenkov counters whose outputs were not used in the analysis reported here.
2. A front-face schematic view of the electromagnetic and the upstream hadronic sections of the calorimeter. In (a) center-of-mass production angles for massless secondaries are shown; in (b) the two limited $\Delta\phi$ apertures, "A" and "B" used to form hardware triggers are shown; in (c) the modules used in the limited polar angle acceptance analysis are indicated; in (d) the module groups used in the modified "two-high" analysis (see text) are shown.
3. Invariant differential cross sections for the production of hadronic clusters in the pseudorapidity range $2.82 < \eta_{LAB} < 3.92$. Only statistical errors are shown; systematic errors are estimated to change the results by approximately ±20% for E_t values greater than 2.5 GeV. The solid line is the result of parametrizing the world data for the single particle production of $\pi^{\pm}$, $K^{\pm}$, p and $\bar{p}$'s (Ref. 13). The dotted line is a fit to single charged particle data (the sum of $\pi^{\pm}$, $K^{\pm}$, p and $\bar{p}$) measured at 90° in the center-of-mass (Ref. 14). The world data parametrization did not include the data from Ref. 14.
4. Hadronic cluster multiplicity distribution. Statistical errors (vertical lines) and systematic uncertainties (horizontal parenthesis) are both shown. The line is a fit to the data reported in Ref. 15.
5. Yields detected in sectors A (triangles, $\Delta\Omega^* = 1.65$ sr) and B (dots, $\Delta\Omega^* = 0.70$ sr) of the calorimeter as a function of transverse energy in the respective sectors. Statistical errors only are shown. The uncertainty in the E_t scale is estimated to be ±5%.

6. A comparison between yields obtained using a hardware trigger (circles) and by applying a software acceptance cut to the global data set (crosses). Only statistical errors are shown. The two sets of data are for a) Sector A ($\Delta\Omega^* = 1.65$ sr) and b) Sector B ($\Delta\Omega^* = 0.7$ sr).
7. Yields obtained by applying software acceptance cut of $2.82 < \eta_{LAB} < 3.92$ to the global data. The circles, full triangles, full squares, open triangles, dots and open squares refer to data obtained with 2π, π, $\pi/2$, $\pi/4$, $\pi/8$ and $\pi/16$ azimuthal acceptances respectively. For reasons of clarity, the results from the π, $\pi/2$, $\pi/4$, $\pi/8$ and $\pi/16$ acceptances have been multiplied by 10^{-1}, 10^{-2}, 10^{-3}, 10^{-4} and 10^{-5} respectively. Only statistical errors are shown. The uncertainty in the E_t scale is estimated to be ±5%.
8. The average hadronic cluster multiplicity detected in the calorimeter. The solid and dotted curves are the predictions of the LPS and QCD models respectively. Statistical errors (vertical lines) and systematic uncertainties (vertical parenthesis) are both shown.
9. The dependence of the average transverse energy of hadronic clusters on the total transverse energy detected in the calorimeter. Statistical errors (vertical lines) and systematic uncertainties (vertical parenthesis) are both shown. The dotted curve is the prediction of the QCD model.
10. Planarity distributions for events with a) medium values of transverse energy ($14 > E_t > 7$ GeV) and b) high values of transverse energy ($E_t > 14$ GeV). The original data (dots) and randomized data (crosses) are both shown.

11.a) Average planarity (calculated using the global data) as a function of transverse energy detected in the total calorimeter. The solid and dotted curves are the predictions of the LPS and QCD models respectively.

b) The fraction of events in the global data set that possess planarity values greater than 0.7 as a function of transverse energy detected in the total calorimeter. The solid and dotted lines are the predictions of the LPS and QCD models respectively.

12. Transverse energy flow as a function of azimuthal angle as measured from the track with maximum transverse energy. The original data (points) and a fit to the randomized data (solid line) are shown. The transverse energy of the maximum E_t track is not included in this plot.

13. The fraction of events with $P > 0.7$ that remain with $P > 0.7$ after randomization. Statistical errors only are shown.

14. Average planarity as a function of E_t for events obtained using a limited $\Delta\phi$ trigger. Planarity was calculated using the responses from all modules; E_t was formed using the responses from triggering modules alone. The solid and dotted curves are the predictions of the LPS and QCD models respectively.

15. Normalized transverse energy flows vs. azimuthal angle as measured from center of the triggering sector. Low ($2 < E_t < 3$ GeV), medium ($4 < E_t < 5$ GeV) and high E_t ($6 < E_t < 8$ GeV) data sets are shown. E_t is the transverse energy detected in the triggering sector alone. The solid and dotted lines are predictions of the LPS and QCD models respectively.

16. The fraction of events with pseudothrust greater than 0.96 as a function of E_t. E_t is the transverse energy detected in the triggering sector.

17. Normalized transverse energy flows for events with high and low pseudothrust values ($T > 0.96$ and $T < 0.96$ respectively). $\phi = 0°$ corresponds to the center of the triggering sector.

18. Planarity distributions for the limited θ^* acceptance global data. The three E_t ranges (6 to 9 GeV, 9 to 12 GeV and 12 to 15 GeV) were calculated using only the responses from the modules within a reduced θ^* aperture.

19. a) The average planarity of events and b) the fraction of high planarity events as a function of E_t calculated using the responses from the modules within a reduced θ^* aperture. The solid and dotted curves are the predictions of the LPS and QCD models respectively.

20. Fraction of events with $E_t > 12$ GeV and with two limited acceptance regions both possessing $E_t > E_t^{thr}$. The solid and dotted curves are predictions of the LPS and QCD models respectively.

21. Average planarity of events with $E_t > 12$ GeV and with two limited acceptance regions both possessing $E_t > E_t^{thr}$. The solid and dotted curves are predictions of the LPS and QCD models respectively.

22. Average planarity (calculated using all calorimeter tracks) for events with low and high hadronic track multiplicity.

23. Average planarity (calculated using all calorimeter tracks) as a function of the total a) electromagnetic and b) hadronic transverse energy detected in the calorimeter. Only statistical errors are shown.

24. Average planarity for events with relatively high values (dots) and medium values (crosses) of a) electromagnetic and b) hadronic transverse energy as a function of the total transverse energy in the calorimeter.

25. The difference in average planarity for events with high and medium values of a) electromagnetic and b) hadronic transverse energy. The E_t ranges used were a) $E_t^{em}/E_t > 0.6$, $0.2 < E_t^{em}/E_t < 0.6$ and b) $E_t^{had}/E_t > 0.8$, $0.4 < E_t^{had}/E_t < 0.8$.

26. Average planarity, calculated using only secondaries with $p_t > 0.5$ GeV/c, as a function of E_t (calculated using all tracks).

27. Fraction of the total E_t that the highest E_t track possesses (crosses) and the pair of highest E_t tracks possesses (circles).

28. Scaled transverse energy distributions for hadronic tracks from high transverse energy events ($E_t > 14$ GeV) with a) low, b) medium and c) high values of planarity. The full curve in c) is e^+e^- data (see Ref. 28); the dotted curve is the prediction of the QCD model. Only statistical errors are shown. Systematic uncertainties are estimated at ±20%.

29. Scaled transverse energy distributions for hadronic tracks from high planarity ($P > 0.7$) events. Distributions for events with $E_t < 7$ GeV (triangles), $7 < E_t < 14$ GeV (crosses) $E_t > 14$ GeV (dots). Only statistical errors are shown.

30. Distributions of the component of hadronic track momenta perpendicular to the "jet" direction. Data from low ($P < 0.3$), medium ($0.3 < P < 0.7$) and high ($P > 0.7$) planarity events are shown. Data are for events with $E_t > 14$ GeV. The full curve is e^+e^- data (see Ref. 29).

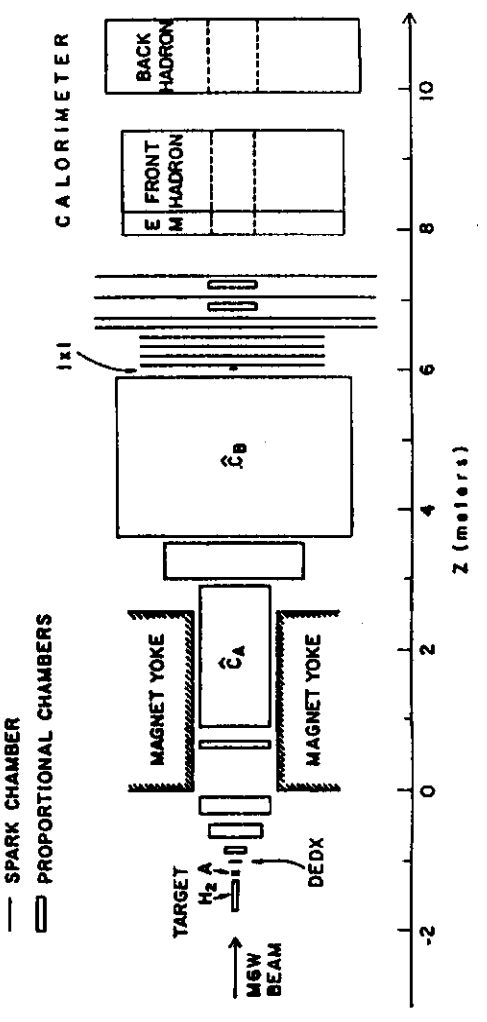

FIG. 1